Potential-Induced Redox Switching in Viologen Self-Assembled Monolayers: An ATR−SEIRAS Approach

B. Han,[†] Z. Li,[†] T. Wandlowski,*[,†] A. Błaszczyk,[‡,§,#] and M. Mayor[‡,⊥]

Institute of Bio- and Nanosystems (IBN 3) and Center of Nanoelectronic Systems for Information Technology (CNI), Research Center Jülich GmbH, D52425 Jülich, Germany, and Institute for Nanotechnology, Research Center Karlsruhe GmbH, P. O. Box 3640, D76021 Karlsruhe, Germany

Received: April 25, 2007; In Final Form: June 18, 2007

Monolayers of viologens (*N*-alkyl-*N*′-(*n*-thioalkyl)-4,4′-bipyridinium bromide, $n = 6, 8, 10$) have been self-assembled from ethanolic solution onto gold substrates. Their structure and redox functionality were studied by cyclic voltammetry and in situ ATR−SEIRAS. Voltammetric experiments revealed that the first redox process, $V^{2+} \leftrightarrow V^{\bullet+}$, is reversible, whereas the second redox process, $V^{\bullet+} \leftrightarrow V^0$, is quasi reversible. The V^{2+} adlayer exhibits a sandwich-like structure. Van der Waals interactions between the alkyl chains lead to two well-ordered hydrophobic layers, with the redox-active bipyridinium unit enclosed in between. The alkyl chains are aligned in an all-trans configuration in a tilted orientation with respect to the surface normal and exhibit a slight conformational disorder. The long axis of the central bipyridinium rings is also tilted. The alignment of V^{2+} is stabilized by interplanar $\pi-\pi$ stacking and electrostatic coulomb interactions. Both monomers and dimers of $V^{\bullet+}$ coexist in the $V^{\bullet+}$adlayer. The molecular alignment of the $V^{\bullet+}$ adlayer is stabilized by the strong vibronic coupling within the dimers and the $\pi-\pi$ stacking between the monomers. Increasing length of the alkyl chain results in more tilted bipyridinium units, and favors both the dimerization and the alignment of $V^{\bullet+}$ within the SAMs. The complex reaction, $V^{2+} \rightarrow V^{\bullet+}$, is described as electron transport from the electrode to the V^{2+} moiety followed by the dimerization of $V^{\bullet+}$, the delocalization of the radical electrons, and the migration of coadsorbed ClO_4^- anions.

1. Introduction

Viologens are obtained by diquaternizing of 4,4′-bipyridine to 1,1′-disubstituted 4,4′-bipyridinium salts.[1] The redox-active bipyridinium centers occur in three different oxidation states: the oxidized dication V^{2+}, the radical cation $V^{\bullet+}$, and the fully reduced neutral form V^0, which may transform into each other in two sequential one-electron processes: $V^{2+} \leftrightarrow V^{\bullet+}$ and $V^{\bullet+} \leftrightarrow V^0$.[1,2] Viologens and their derivatives have been used in various applications such as functional polymers,[3−5] biosensors,[6−8] liquid crystals,[9] photo energy conversion,[10] complex-stabilized metal particles,[11] and luminescent materials.[12] Recently, viologens were also incorporated as functional "backbone components" in self-assembled monolayers (SAM),[13,14] Langmuir−Blodgett films,[15,16] nanometer-scale electronic switches, and various novel materials[17−20] employing the precise control of their redox state upon electrochemical polarization.

The self-assembly and redox-functionality of viologens on solid electrodes (Au, Ag, Pt, HOPG, etc.) have been widely investigated by cyclic voltammetry,[20−43] UV−vis-absorption,[42−45] vibrational spectroscopy (IR and Raman),[13,31−37,42−52] quartz crystal microbalance,[21−23,53,54] electroreflectance,[24−30] STM,[14] and STS.[13] The solution-based electrochemical studies provide important clues for understanding the properties of surface-immobilized viologen monolayers. For example, the thermodynamic redox potentials are strongly dependent on the hydrophobic/hydrophilic environment which is controlled by the length of the alkyl chains,[21−23,38−40,42,43] and the interactions between bipyridium centers and coadsorbed anions.[21−27,31−37]

Intrinsic structures and chemical changes were, in particular, investigated by various vibrational spectroscopy techniques in combination with electrochemical measurements. Both IR and Raman spectroscopic studies demonstrated the coexistence of monomer and dimer radical cations in viologen adlayers.[31−37,44−46,49−50] The equilibrium between monomer and dimer radical cations, their dependence on coadsorbed anions and on the length of the alkyl chains were characterized in detail.[31−37,42−45] Surface enhanced infrared absorption spectroscopy (SEIRAS), a recently developed IR technique, was applied to explore structure details with focus on the real-time monitoring of interfacial electrochemical reactions. Osawa et al. studied the electrodeposition of heptylviologen cations on Ag electrodes.[47,48] They found clear evidence for a face-to-face sandwich structure of the radical dimers. The radical electrons are delocalized over the whole bipyridinium cores giving rise to strong spin-pair interactions.[47,48,51,52] However, a systematic SEIRAS characterization of self-assembled viologen monolayers is not yet available. Important topics, such as the role of the counter anions during the redox reactions and the nature of the "electrochemical switching"[55] processes between the different redox states, have not been addressed.

Motivated by recent investigations on the single molecule conductance of viologen-based molecular junctions,[56,57] we explored the relations between molecular structure and electronic

* Corresponding author e-mail: th.wandlowski@fz-juelich.de.
[†] Research Center Jülich GmbH.
[‡] Research Center Karlsruhe GmbH.
[§] Home address: Faculty of Commodity Science, Al. Niepodlegloci 10, 60–967 Poznań, Poland.
[⊥] Also Department of Chemistry, University of Basel, St. Johanns-Ring 19, CH-4056, Basel, Switzerland.
[#] Also Department of Chemistry and Biochemistry, University of Berne, Freiestrasse 3, CH-3012 Bern, Switzerland.

10.1021/jp073208g CCC: $37.00
Published on Web 08/29/2007

SCHEME 1: Molecular Structure and Redox Reactions of Viologen

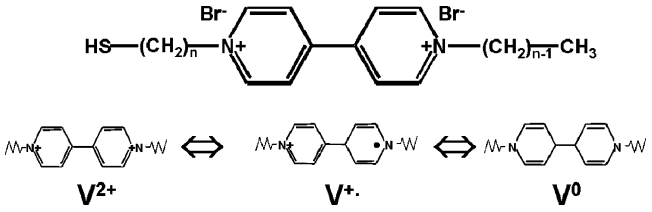

properties from macroscale self-assembled viologen monolayers to single-molecular junctions employing an STM-based approach.[58,59] Complementary to this work, we report in this article a detailed in situ SEIRAS study of structure and chemical functionality of self-assembled viologen monolayers immobilized on electrified gold/electrolyte interfaces employing an attenuated total reflection (ATR) configuration.

2. Experimental Section

2.1. Preparation. *2.1.1. Synthesis.* The synthetic strategy to obtain the *N*-alkyl-*N*′-(*n*-thioalkyl)-4,4′-bipyridinium bromide derivatives with $n = 6$, 8, and 10 is based on a nucleophilic substitution reaction between pyridines and terminal alkylbromides. Details of the preparation and purification were reported in refs 58 and 59. As illustrated in Scheme 1, each viologen molecule is composed of a redox-active bipyridinium center, two flexible alkyl spacer units, and one terminal thiol anchor group. Depending on the number of CH_2 units in the alkyl chains, the viologen derivatives are labeled 6V6, 8V8, and 10V10 for $n = 6$, 8, and 10, respectively.

2.1.2. SAM Preparation. In electrochemical measurements, island-free Au(111)-(1 × 1) single-crystal electrodes were used as substrates for viologen self-assembly. The unreconstructed surfaces were achieved by immersing freshly flame-annealed electrodes into deaerated 0.1 M HCl under potential control at 0.500 V (vs SCE) to lift the surface reconstruction, then thoroughly rinsed with Milli-Q water to remove Cl^-.[66] In IR experiments, electron-beam evaporated Au films on Si surfaces were directly used as the quasi-Au(111) substrates without any further surface treatment.

The viologen monolayers were prepared by immersion of the gold electrodes in ethanolic (p.a. KMF) solutions of the respective molecules, followed by thermal annealing at 60 °C for 6 h to create ordered high-coverage monolayers. The concentration of viologen in ethanol was 1.0 mM for Au(111) single crystals, and 0.5 mM for Au(111-25 nm) film electrodes. The formation and characterization of the adlayers were carried out in the strict absence of oxygen. The thermal treatment was performed in a stainless steel autoclave to prevent the evaporation of ethanol.

After the self-assembly, the modified Au-electrodes were rinsed with warm ethanol to remove physisorbed viologen species, subsequently dried in a stream of argon, followed by mounting into the electrochemical or spectroelectrochemical cells.

2.2. Electrochemistry. The supporting electrolyte was an alkaline aqueous solution of 0.05 M $KClO_4$ prepared with Milli-Q water (18 MΩ, 2∼3 ppb TOC), $KClO_4$ (Fluka puriss. p.a., twice recrystallized from water), and NaOH (suprapure, Merck). The glassware was cleaned either in a hot 1:1 mixture of H_2SO_4 and HNO_3, or by soaking in caroic acid. All electrolytes were deareated with 5 N argon before and during the experiments. The measurements were carried out at 20 ± 0.5 °C.

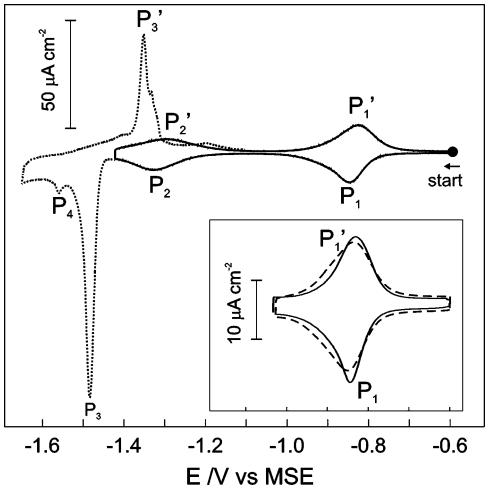

Figure 1. Current−potential curves (CV) of a 6V6 monolayer on Au(111)-(1 × 1) in 0.05 M $KClO_4$, pH ∼ 10. Contact with the electrolyte was established at $E = -0.600$ V; potential sweep rate 50 mV s^{-1}. Solid line: reversible CV recorded in -1.400 V $< E < -0.600$ V; dotted line: first voltammetric cycle measured in -1.650 V $< E < -0.600$ V. The inset illustrates the one-electron reaction for $V^{2+} \leftrightarrow V^{+\cdot}$ of a 6V6 SAM on a Au(111) single-crystal electrode (solid line) and on a Au(111−25 nm) film electrode (dashed line) in 0.05 M $KClO_4$, pH ∼ 7. All CVs started at −0.600 V.

The electrochemical measurements were performed in lab-built three-electrode cells employing an AutoLab (PGSTAT-30) potentiostat. The counter electrode was a platinum wire, and a mercury sulfate electrode (MSE) served as reference. All potentials in this paper are quoted with respect to this electrode.

2.3. Spectroelectrochemistry (ATR−SEIRAS). The SEIRAS experiments were carried out in a vertical spectroelectrochemical cell in a Kretschmann ATR-configuration.[61−63] The electrode potential was controlled and synchronized with a HEKA (PG 310) potentiostat.

The infrared spectra were measured with a Bruker IFS66 v/S Fourier Transform IR spectrometer. The spectral resolution was 4 cm^{-1}. IR radiation from a globar source was p-polarized and focused onto the electrode/electrolyte interface by passing through the back of a hemispherical Si prism. The incident angle was typically 70° referred to the surface normal. The IR radiation totally reflected at the interface was measured with a liquid-nitrogen cooled MCT detector (Model Colmar Technologies MCT 317).

2.4. In Situ STM. The in situ STM experiments were carried out with a Molecular Imaging Pico-SPM on disc-shaped Au(111) massive single-crystal electrodes. The STM tips were electrochemically etched W tips (0.25 mm diameter), coated with polyethylene. Pt wires served as reference and counter electrodes. All STM images were recorded at room temperature in constant current mode with tunneling currents ranging between 3 and 200 pA. Details of the STM setup were described in refs 58 and 59.

3. Results and Discussion

3.1. Cyclic Voltammetry. The viologen adlayers on single-crystal Au(111) electrodes were first characterized by cyclic voltammetry. Figure 1 shows typical voltammograms of a Au(111)-(1 × 1) electrode modified with a monolayer of 6V6 in contact with 0.05 M aqueous $KClO_4$, the pH value of which was adjusted to ∼10 by adding NaOH. Restricting the potential range to -1.400 V $< E < -0.600$ V results in two pairs of well-resolved current peaks $P_1(-0.850\text{ V})/P_1'(-0.820\text{ V})$ and $P_2(-1.330\text{ V})/P_2'(-1.300\text{ V})$ (solid line), which represent the

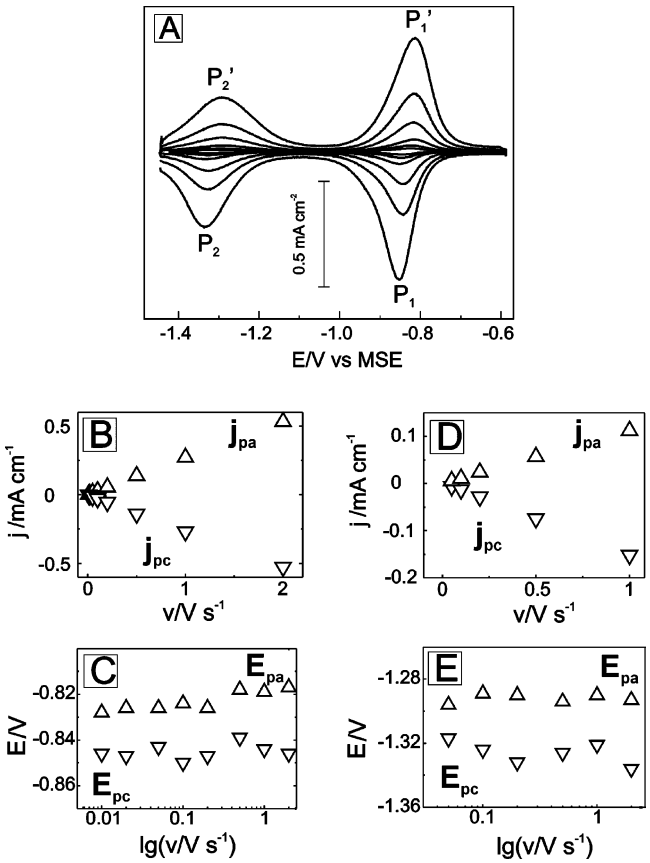

Figure 2. (A) CVs of a 6V6 SAM on a Au(111)-(1 × 1) in 0.05 M $KClO_4$, pH ~ 10, as recorded with different scan rates ranging between 10 mV s^{-1} and 2 V s^{-1}; (B, C) Scan rate dependencies of the peak current densities (j_{pa}, j_{pc}), and of the peak potentials (E_{pa}, E_{pc}) for the first redox process. (D, E) Scan rate dependencies of the peak current densities (j_{pa}, j_{pc}), and of the peak potentials (E_{pa}, E_{pc}) for the second redox process. The anodic and cathodic scan directions are labeled as (△) and (▽). The solution resistance was compensated by applying a positive feedback.

characteristic first ($V^{2+} \leftrightarrow V^{\bullet+}$) and second ($V^{\bullet+} \leftrightarrow V^0$) redox processes of the viologen moiety.[1] Further details of the two electrode reactions can be revealed by recording voltammograms with different scan rates.[64] Figure 2A shows selected data for 10 mV s^{-1} up to 2 V s^{-1}.

3.1.1. First Redox Process: $V^{2+} \leftrightarrow V^{\bullet+}$. The peak currents scale linearly with scan rate (Figure 2B), and the peak-to-peak separations of P_1/P_1' are constant up to 2 V s^{-1} (Figure 2C). The fwhm is 0.091 V for both P_1 and P_1'. These observations indicate a reversible process in which the redox-active species are confined to the electrode surface.[64]

The formal potential $E^{0\prime}$ (estimated as the midpoint between the anodic and the cathodic peak potentials) is more negative than the values reported for Cl^-, Br^-, and SO_4^{2-} containing electrolytes.[21−23,31−37] These observations indicate a possible exchange of the hydrophilic Br^- anions by the hydrophobic ClO_4^- anions in 0.05 M $KClO_4$. ClO_4^- is known to interact strongly with the V^{2+} dications, and may permeate through the alkyl chains to reach the redox centers due to its rather small hydrated diameter.[21−23] The incorporation of ClO_4^- is also suggested by the rather large adlayer capacitance, $C_{dl} = 8.8\ \mu F\ cm^{-2}$, as compared to typical values of alkanethiol monolayers.[65] The migration of ClO_4^- will be investigated in detail by in situ ATR−SEIRAS.

The nonnegligible peak-to-peak separation $\Delta E_p \sim 20$ mV (Figure 2C) indicates some complexity of the "reversible" ET process. Contributing processes may involve changes in the solvation shell as well as substantial electrostatic interactions.[21−23,66] Specifically, we mention the effect of ion pairing,[67−69] which results from strong electrostatic interactions between the V^{2+} centers and the hydrophobic ClO_4^- anions. The formation of ion pairs was also reported for electron-transfer processes with ferrocene derivatives in 1.0 M $HClO_4$ immobilized on gold electrodes.[70,71]

A systematic STM study revealed a densely packed monolayer of 6V6 on Au(111) single-crystal electrodes.[58,59] We estimated a consumed charge of ~30 μC cm^{-2} by integrating the current vs potential curve of the first pair of peaks P_1/P_1' and considering a one-electron-transfer process ($V^{2+} \leftrightarrow V^{\bullet+}$). This value corresponds to a surface coverage of approximately $(3.5 \pm 0.3) \times 10^{-10}$ mol cm^{-2} (~47 $Å^2$ per molecule), and is in good agreement with literature data reported for related systems (41 ~ 55 $Å^2$).[20−23,44,45,72] However, it is significantly smaller than the projected area of a planar oriented 6V6 molecule (estimated from crystal structure data in refs 73 and 74), but larger than the estimated cross section of an all-trans oriented alkanethiol in a densely packed SAM (18 ~ 20 $Å^2$).[75] This qualitative discussion suggests a tilted orientation of the viologen moiety with respect to the surface normal. A similar hypothesis was also reported by Sagara et al. based on electroreflectance studies.[24−27]

3.1.2. Second Redox Process: $V^{\bullet+} \leftrightarrow V^0$. The peak heights scale linearly with the scan rate (Figure 2D). A decay in the peak current of P_2/P_2' was observed after long-time potential cycling in $-1.430\ V < E < -1.100$ V. The peak-to-peak separations ΔE_p of P_2/P_2' are rather constant (~32 mV) for scan rates up to 1 V s^{-1} (Figure 2E). Compared to $V^{2+} \leftrightarrow V^{\bullet+}$ (P_1/P_1'), the reaction $V^{\bullet+} \leftrightarrow V^0$ (P_2/P_2') appears to be less reversible under our experimental conditions, as indicated by larger fwhm values. The large values of the fwhm [0.110 V (P_2) and 0.132 V (P_2')] suggest a certain disorder within the adlayer, which could be related to the penetration of anions, the uneven distribution of the redox centers, or the aggregation of different $V^{\bullet+}$ species.[66] The lower reversibility of the second process $V^{\bullet+} \leftrightarrow V^0$ is partially attributed to the insolubility and/or aging tendency of the V^0 species,[46,66] which generate an additional heterogeneity within the adlayer. This explanation is supported by the uneven charge balance between the negative going (P_2) and the positive going (P_2') sweeps. The former is significantly larger than the latter.

3.1.3. Reductive Desorption. Potential excursion to more negative values reveals a pair of sharp current peaks P_3(−1.480 V) and P_3'(−1.350 V) (Figure 1, dotted line), which are assigned to the irreversible reductive desorption of the chemisorbed 6V6 adlayer, and the partial oxidative readsorption of redox-active thiolates.[76,77] Current integration of P_3, after correction of the double layer contribution, yields an effective desorption charge of 160 ± 10 μC cm^{-2}, which is considerably larger than (i) the charge estimated for a 6V6 monolayer based on the integration of P_1/P_1' (~ 30 μC cm^{-2}) as well as (ii) typical values of reductive desorption reported for alkanethiols (~ 70 μC cm^{-2}).[65] This comparison demonstrates that parallel contributions from additional faradaic processes are involved.[28−30,66]

3.1.4. Dependence on the Alkyl Chain Lengths. Figure 3 shows the cyclic voltammograms of the first redox process ($V^{2+} \leftrightarrow V^{\bullet+}$) for 6V6, 8V8, and 10V10 SAMs. The current−potential characteristics of 8V8 and 10V10 show similar symmetric and reversible first redox peaks P_1/P_1', and also rather similar values

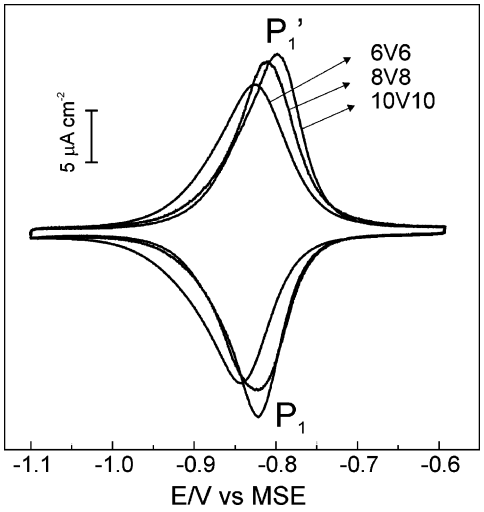

Figure 3. CVs of the first redox step of 6V6, 8V8, and 10V10 SAMs on Au(111)-(1 × 1) single-crystal electrodes in 0.05 M $KClO_4$, pH ~ 10, scan rate 50 mV s^{-1}.

TABLE 1: CV Parameters of Viologen SAMs with Different Alkyl Chain Lengths (First Redox Process); (a) Anodic Scan and (c) Cathodic Scan

	ΔE_p (V)	peak potential (V)	$E^{0\prime}$ (V)	fwhm (V)	Γ ($\times 10^{-10}$ mol cm^{-2})	desorption potential (V)
6V6	0.020	−0.825 (a)	−0.835	0.103 (a)	3.31	−1.480
		−0.845 (c)		0.097 (c)		
8V8	0.018	−0.807 (a)	−0.816	0.092 (a)	3.42	−1.490
		−0.825 (c)		0.080 (c)		
10V10	0.017	−0.801 (a)	−0.809	0.084 (a)	3.51	−1.480
		−0.818 (c)		0.077 (c)		

of the adlayer capacitance (C_{dl} ~ 9.0 μF cm^{-2}) as 6V6. Characteristic parameters of the data analysis are summarized in Table 1.

The peak currents increase and the fwhm decrease slightly with the length of the alkyl chain. The estimated surface coverage increases in the following sequence: 6V6 < 8V8 < 10V10. Longer alkyl chains exhibit stronger van der Waals interactions, which result in an improved two-dimensional order within the adlayer. Similar observations were also reported for alkanethiol SAMs.[66,75] Considering the increase of the spatial size along the alkyl chain axis with increasing number of CH_2 units, the surface coverage should have decreased according to 6V6 > 8V8 > 10V10 if the molecules were aligned parallel to the substrate. However, the reversed trend indicates a tilted orientation of the viologen molecules within the SAM as spatial increase for longer alkyl chains occurs only along the chain axis.

The anodic and cathodic peak potentials shift toward positive values with increasing alkyl chain length, i.e., with increasing distance between the redox moiety and the monolayer/solution interface. V^{2+} is hydrophilic and hydrated, while $V^{\bullet+}$ is hydrophobic. Long alkyl chains provide a hydrophobic environment, which favors the $V^{\bullet+}$ rather than the V^{2+} species. Therefore, the prevailing $V^{\bullet+}$ will push the $V^{2+}/V^{\bullet+}$ equilibrium potential to more positive values.[21−23] A similar positive potential shift was observed for ferrocenylalkane thiols.[70]

The average fwhm values of the current peaks decrease with increasing alkyl chain lengths, indicating that the attractive interactions within the adlayer are enhanced.[71] Such attractive interactions may originate from ion-pairing interaction,[21−23] together with π-stacking between the bipyridinium planes and strong van der Waals interactions between neighboring alkyl chains in an all-trans conformation.

Within the experimental error, the peak-to-peak separations between the cathodic and the anodic peaks are constant (~ 19 mV) for viologen with different alkyl chain lengths. Such an independence of ΔE_p on the alkyl chain length indicates that the first redox process is dominated by the redox centers themselves and their local solvent/anion environment.

3.1.5. Au(111−25 nm) Film Electrodes in Neutral Solution. The SEIRAS measurements were carried out with quasi single crystalline Au(111−25 nm) film electrodes to characterize structural changes within the viologen adlayer during the redox process $V^{2+} \leftrightarrow V^{\bullet+}$.[61,78] The dashed line in the inset of Figure 1 represents the CV of a Au(111−25 nm) film electrode modified with 6V6 at pH ~ 7. The data are in good agreement with results obtained for 6V6 adlayers on massive single crystalline Au(111)-(1 × 1) electrodes at pH ~ 7 (Figure 1 inset, solid line). The larger adlayer capacitance (~11.5 μF cm^{-2}) and the lower surface coverage (~ 3.09 × 10^{-10} mol cm^{-2}) are due to the imperfect morphology of the film electrode. In consequence, the adlayer is less uniform, and additional solvent molecules are incorporated.[61,63]

Based on the above similarities between massive single crystalline and film electrodes, the IR investigations of the first redox process of the viologen SAMs can be reliably carried out in neutral solution on modified Au(111−25 nm) film electrodes.

3.2. ATR−SEIRAS. Cyclic voltammetry provides an understanding of the overall redox properties and of the general stability of the viologen adlayers on massive and thin film gold electrodes. However, molecular structure and chemical composition of these redox-active SAMs as well as the local environment (anions, solvent molecules) are not directly accessible. These aspects will be addressed in a comprehensive in-situ ATR−SEIRAS study on the steady state and dynamic properties of V^{2+} respective of $V^{\bullet+}$ adlayers on Au(111−25 nm) film electrodes.

3.2.1 Steady-State V^{2+} Structure. We investigated first the steady-state structure properties of the V^{2+} adlayer. Figure 4 shows typical ATR−SEIRA spectra of 6V6, 8V8, and 10V10 SAMs in 0.05 M $KClO_4$ at −0.600 V. The reference spectrum was taken at the same potential for the bare gold electrode. Three main regions of viologen-related vibration modes are observed at 1000~1750 cm^{-1}, 2800~3000 cm^{-1}, and 3000~3100 cm^{-1}. They correspond to the ring vibrational modes of the bipyridinium planes, the C−H stretching vibrations of the alkyl chains, and the in-plane aromatic C−H stretching vibrations of the bipyridinium rings, respectively. In addition, the symmetric Cl−O stretching mode of ClO_4^- ($\nu_{(Cl-O)}$), the HOH-bending modes ($\delta_{(HOH)}$), and the broad OH-stretching modes ($\nu_{(O-H)}$) of coadsorbed water species are observed at 1100 cm^{-1}, 1650 cm^{-1}, and 2800~3600 cm^{-1}, respectively. Their dependencies on the different intermolecular interactions are separately discussed in the following sections.

3.2.1.1. Ring Vibration Modes. The vibration bands of the bipyridinium ring below 1750 cm^{-1} are assigned to in-plane dipole moment components either parallel to the long molecular axis, as defined in the inset of Figure 4 by the 4,4′-*N*,*N*′-direction (B_{3u} in D_{2h} symmetry: 1642, 1508, 1225, 1180 cm^{-1}), or parallel to the short molecular axis (B_{2u} modes in D_{2h} symmetry: 1450, 1355, 1280 cm^{-1}).[46,51,52,79−83] They are superimposed with the $\delta_{(HOH)}$ bands of interfacial water.

Referring to the surface selection rule of SEIRAS, the observation of the B_{2u}, B_{3u} ring vibrations and the aromatic C−H

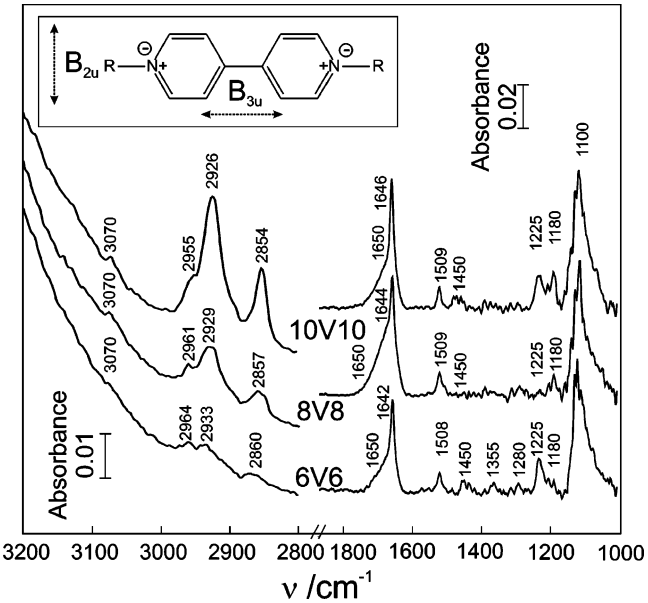

Figure 4. In situ SEIRA spectra of 6V6, 8V8, 10V10 SAMs on Au(111−25 nm) electrodes recorded at $E = -0.600$ V in 0.05 M $KClO_4$, pH ∼ 7. The background spectrum was obtained in the absence of viologen in bare 0.05 M $KClO_4$, pH ∼ 7, at $E = -0.600$ V. Each spectrum was obtained from the average of 256 interferograms after baseline correction. The inset illustrates schematically the molecular structure of V^{2+}. The B_{3u} and B_{2u} axis correspond to the long and short molecular axis of bipyridinium center, respectively.

stretching modes indicates a tilted orientation of both the long and the short axis of the coplanar bipyridinium moiety with respect to the surface normal. Support for this conclusion is provided by recent results with similar systems. Sagara et al. concluded, based on electroreflectance experiments, that the long axis of the bipyridinium group in 4V4, assembled on a polycrystalline Au electrode exhibits an orientation angle of 70° with respect to the surface normal.[24−27] Based on a combined IR and near edge X-ray absorption fine structure spectroscopy study, Rong et al. reported tilt and lean angles of 45° and 70° for the aromatic moiety in monolayers of 4-methyl-4′(*n*-mercaptoalkyl)biphenyls with an even number of methylene groups on Au(111).[84]

3.2.1.2. C−H Stretching Modes of Alkyl Chains. The vibrational bands in 2800∼3000 cm^{-1} (Figure 4) can be assigned to the C−H stretching vibrations of the CH_3 asymmetric ($\nu_{a(CH3)}$ at 2964 cm^{-1}), the symmetric ($\nu_{s(CH3)}$ at 2890 cm^{-1}), the CH_2 asymmetric ($\nu_{a(CH2)}$ at 2933 cm^{-1}), and the symmetric ($\nu_{s(CH2)}$ at 2860 cm^{-1}) stretching modes.[51,52,80,81] This assignment agrees with the absence of $\nu_{a(CH3)}$ and $\nu_{s(CH3)}$ modes in the spectra of dithiol viologen HS-6V6-SH as reported in refs 58 and 59. The analysis of the intensity ratio of $\nu_{a(CH2)}$ to $\nu_{s(CH2)}$ supports a tilted orientation for the alkyl chains with respect to the surface normal.[85,86] The tilted angle can be estimated to be approximately 20−30°.[24−27]

The positions of the methylene C−H stretching modes provide a measure of the intermolecular environment of the alkyl chains in the molecular assembly. The peak frequencies of $\nu_{s(CH2)}$ and $\nu_{a(CH2)}$ in the liquid state are typically higher than those for highly ordered crystalline polymethylene chains (2858 vs 2850 cm^{-1}, 2930 vs 2920 cm^{-1}).[85] Referring to the results of Porter et al., the methylene chain environment of the high coverage 6V6 SAM is liquid-like, i.e., there exists a considerable degree of conformational disorder in the 2D arrangement of the alkyl chains.[85]

3.2.1.3. Vibration Mode of ClO_4^- Counter Anions. In addition to the ring vibration bands, a prominent peak appears at 1100 cm^{-1}, which is attributed to the $\nu_{(Cl-O)}$ mode of ClO_4^- anions,[78] which replace the original Br^- anions and are incorporated into the adlayer lattice. These findings support our previously proposed hypothesis, which was based on macroscopic electrochemical measurements.

The replacement of Br^- or Cl^- anions in SAMs of thiol-functionalized viologens by anions with a smaller dynamic hydration sphere, such as ClO_4^- and PF_6^-, was also suggested by Buttry[21−23] and Sagara[24−27] based on cyclic voltammetric experiments. The presence of the hydrophobic ClO_4^- anions increases the 2D order within the organic film as derived from the peak intensities of the B_{3u} modes.[24−27,46] The lower electron donor ability of ClO_4^- reduces the charge transfer between the viologen moiety and the coadsorbed anion.[74] Consequently, a higher π-electron density is kept in the bipyridinium unit,[1] and favors the interplanar $\pi-\pi$ alignment.

3.2.1.4. Influence of the Alkyl Chain Length. The dependence of the V^{2+} adlayer structure on the alkyl chain length is predominantly determined by the lateral interactions (van der Waals) between the neighboring alkyl chains in the SAM. A similar dependence was observed for biphenyl systems.[84]

With increasing number of methylene units, the intensities of the CH_2 and CH_3 stretching modes increase simultaneously. However, their intensity ratio is almost constant, indicating that the orientation of the alkyl chains is independent of the chain lengths. On the other hand, their frequencies shift to lower values (from 6V6 to 10V10, $\Delta\nu = 3\sim6$ cm^{-1} per $(CH_2)_2$), showing a more uniform alignment of the alkyl chains in an all-trans conformation within the assembled viologen SAMs.

Both the intensity and the frequency of the B_{3u} ring mode around 1642 cm^{-1} increase with alkyl chain lengths. Referring to similar coverages of 6V6, 8V8, and 10V10, the higher intensities of the B_{3u} bands of 10V10 can be explained by a more tilted orientation of the $N-N'$ axis, which favors again a stronger $\pi-\pi$ alignment of the bipyridinium planes and thus results in a blue shift. The long alkyl chains not only increase the alignment of the all-trans hydrocarbon chains, but also stabilize the bipyridinium planes by providing a well-defined nonpolar environment, which favors the replacement of Br^- by hydrophobic ClO_4^-.

3.2.1.5. *Model of the V^{2+} Monolayer.* Based on the above qualitative discussion on the structure of the viologen adlayers, we suggest the following model of the V^{2+} SAM (Figure 5). The alkyl chains are aligned in an all-trans conformation along the surface normal in a tilted orientation. The long axis of the central bipyridinium rings is tilted with respect to the surface normal. Van der Waals interactions between the long alkyl chains lead to two well oriented hydrophobic layers, with the redox-active bipyridinium V^{2+} moiety aligned in between. The positive charges of the bipyridinium dications are balanced by the negatively charged anions (initially Br^-, which is replaced by ClO_4^- in aqueous 0.05 M $KClO_4$) located close to the nitrogen atoms. The organization of the bipyridinium dications is stabilized by interplanar $\pi-\pi$ and Coulombic interactions.

The above model is consistent with our previous in-situ STM results of the high coverage 6V6 SAM on Au(111) where an expanded hexagonal monolayer covers the entire substrate surface with a $(\sqrt{7} \times \sqrt{7})$ repeat motif.[58,59] The resulting coverage amounts to 3.3×10^{-10} mol cm^{-2}, which is in good agreement with values estimated from cyclic voltammetry. The open structure is expected due to the bulky size of the tilted viologen moiety which prevents the typical $(\sqrt{3} \times \sqrt{3})$

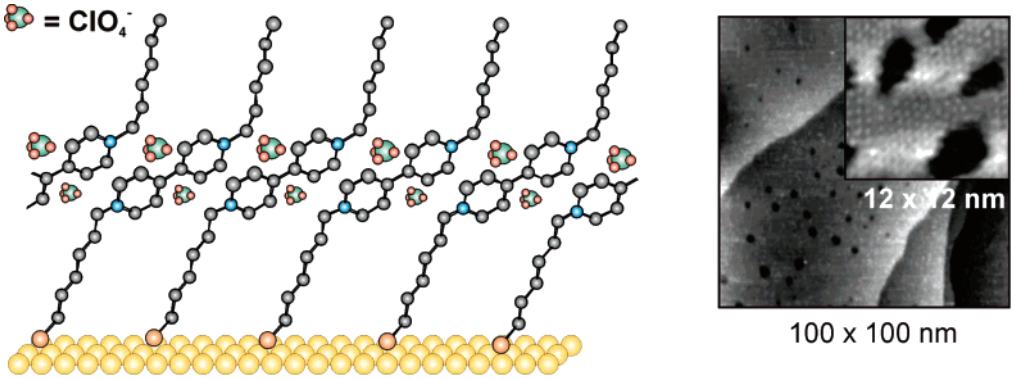

Figure 5. Model of the V^{2+} SAM on a gold surface. The STM image illustrates the structure of a 6V6 SAM on Au(111)-(1 × 1) in 0.05 M $KClO_4$, pH 7, recorded at $E_s = -0.60$ V.

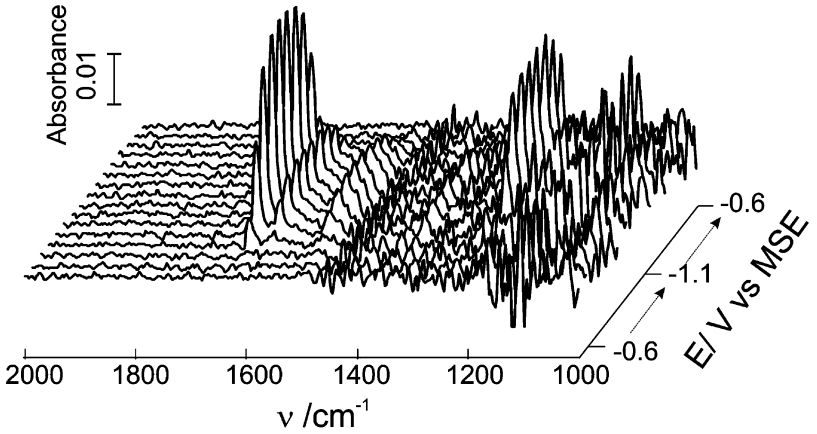

Figure 6. 3D potentio-dynamic SEIRA spectra of a 6V6 SAM on a Au(111−25 nm) film electrode. The spectra were recorded during a potential cycle of 50 mV s^{-1} in -1.100 V < E < -0.600 V (first redox process). The reference spectrum was measured at $E = -0.600$ V. Each potential-difference spectra is the average of 80 interferograms corresponding to a potential resolution of 62 mV.

arrangement. The latter is often observed for high coverage adlayers of alkanethiols on Au(111) electrodes.[87−89]

3.2.2. Quasi-Steady-State Structure of $V^{\bullet+}$. *3.2.2.1. Dynamic SEIRAS.* As shown in Figure 1, the excursion of the electrode potential from $E = -0.600$ V to $E = -1.100$ V triggers the reversible one-electron reduction from V^{2+} to $V^{\bullet+}$. The radical cation $V^{\bullet+}$ can be stabilized by holding the substrate potential at -1.100 V. However, long-term "aging" effects and/or the formation of insoluble salts decrease the stability of the adlayer.[2,28−30,46] Therefore, we focus on the quasi-steady-state SEIRAS spectra of $V^{\bullet+}$ measured in a potential cycle, with the reference spectrum acquired at -0.60 V, where a stable V^{2+} adlayer exists.

A 3D representation of the potentio-dynamic SEIRA spectra of a 6V6 adlayer on a Au(111−25 nm) film electrode is plotted in Figure 6. The reversible evolution of the IR bands in the range of the ring vibrations for $V^{2+} \leftrightarrow V^{\bullet+}$ agrees with the conclusions drawn from cyclic voltammetry. The spectrum recorded at -0.940 V, which represents the quasi-steady-state response of the reduced $V^{\bullet+}$ form, was selected and presented in Figure 7, together with the potential difference spectra of 8V8 and 10V10 recorded under identical conditions at -0.940 V.

Rarely detectable changes appear in the spectra ranges of the $\nu_{(C-H)}$ and $\nu_{(O-H)}$ stretching modes (not shown), illustrating rather similar structures of the alkyl chains in both redox states, and very little reorganization in the structure and amount of interfacial water, respectively. The latter is consistent with the previous expectation of a hydrophobic and compact monolayer, which is stabilized by strong van der Waals interactions between aligned alkyl chains.

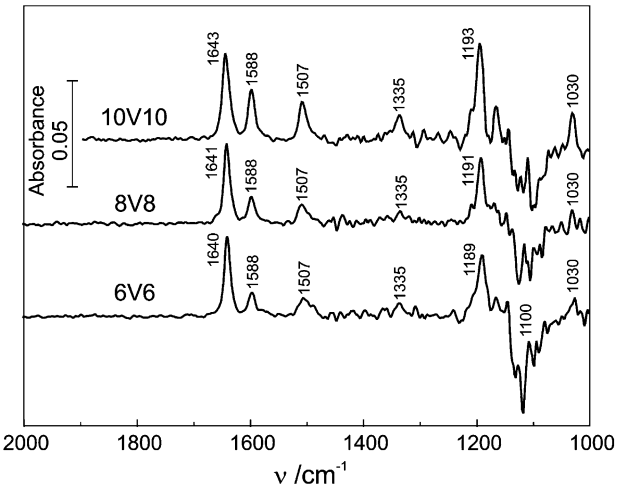

Figure 7. In situ SEIRA spectra of the radical cations ($V^{\bullet+}$) of 6V6, 8V8, and 10V10 SAMs recorded at -0.940 V. The reference spectrum was measured at $E = -0.600$ V. Each potential difference spectrum is obtained from the average of 80 interferograms.

Compared with the featureless high wavenumber range, several positive bands develop at 1640, 1588, 1507, 1335, 1189, and 1030 cm^{-1}. An additional negative-going band appears around 1100 cm^{-1}. They are attributed to the ring vibrational modes of $V^{\bullet+}$ and the symmetric $\nu_{(Cl-O)}$ mode of ClO_4^-, respectively. The presence of such pronounced vibrational bands in the potential difference spectra indicates considerable structure changes in the redox center upon reduction.

The prominent bands at 1640 and 1189 cm^{-1} can be assigned to the asymmetric in-plane ring vibrations of the monomer

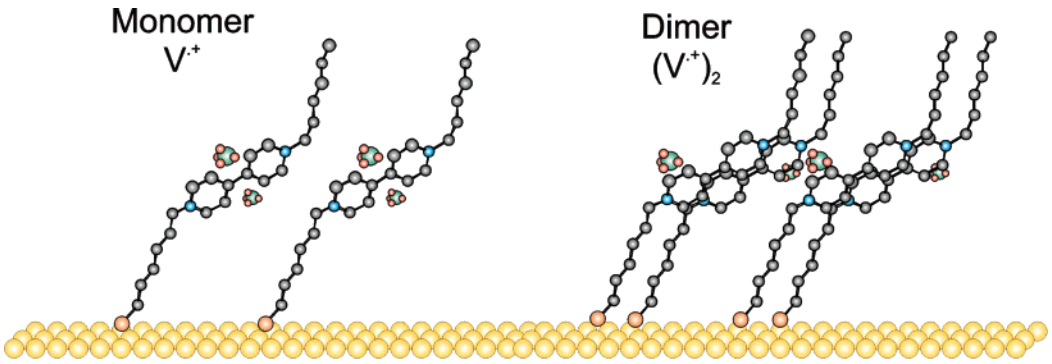

Figure 8. Models of the coexisting monomer and dimer of radical cations in the 6V6 SAM.

radical cation $V^{\bullet+}$. Specific coordination analysis shows that they have the same origin as V^{2+}: the two B_{3u} modes in a D_{2h} symmetry have main contributions from the push−pull movements of the central C−C (1640 cm^{-1}) and the N−R (1189 cm^{-1}) bonds.[46,51,52] Their high intensities can be explained by the enhanced dipole changes originating from the oscillation of the delocalized radical electron between the two pyridine rings, which is parallel to the long molecular axis in $N-N'$ direction. Such oscillation of the delocalized radical electrons suggests an extended aromatic character across both rings, which may partially contribute to the enhancement of the ET through the whole redox center. In this context, we recall that STM-based experiments on single-molecular junction (Au_{tip}-S-6V6-S-$Au_{substrate}$) revealed a 50% higher conductance for the $V^{\bullet+}$ state compared to V^{2+}.[58,59]

The other modes (1588, 1507, 1335, and 1030 cm^{-1}) are attributed to "charge−transfer activated", totally symmetric (A_g) ring vibrations of the radical cation dimer $(V^{\bullet+})_2$. The activation of these A_g modes involves a "vibronic coupling" mechanism in a one-dimensional charge−transfer complex: when two radical $V^{\bullet+}$ planes are linked face-to-face via π-bonding, their individual A_g modes are coupled out-of-phase and activated by a charge polarization, which is induced by the charge−transfer between the two bipyridine units.[79] Therefore, the dipole transitions involved in the vibrational modes of the dimer are normal to the $V^{\bullet+}$ planes.

The $(V^{\bullet+})_2$ dimer is more stable than the monomer because the $\pi-\pi$ stacking interactions between radical planes are stronger than the electrostatic attractions between the radical cation and the attached anions.[46] In spite of the higher stability of the $(V^{\bullet+})_2$ dimer, the radical cation monomer is stabilized by electrostatic attraction with coadsorbed ClO_4^- anions,[21−27,31−37] as well as by the commensurability matching of intra-assembly planes.[75,90,91] Consequently, monomers and dimers of the $V^{\bullet+}$ radical cations coexist in the reduced 6V6 monolayer.

The broad negative-going band around 1100 cm^{-1} indicates the release of ClO_4^- upon the reduction $V^{2+} \rightarrow V^{\bullet+}$, which is also supported by EQCM experiments.[53,54] Due to the smaller hydration shell of ClO_4^- and the hydrophobic character of the alkyl chain environment, the anion migration involves very small amounts of solvent molecules (H_2O). This phenomenon is further reflected in the absence of a $\nu_{(O-H)}$ feature related to the change of interfacial water species in the potential difference spectra between V^{2+} and $V^{\bullet+}$.

3.2.2.2. Alkyl Chain Length Dependence. The lateral interactions can be further addressed by exploring the dependence of the $V^{\bullet+}$ spectra on the length of the alkyl chains. Figure 7 shows selected SEIRA spectra of 6V6, 8V8, and 10V10 measured at −0.940 V. The reference potential was chosen at −0.600 V.

The ring-vibrational modes of the monomers shift to higher wavenumbers with the increase of chain length (from 1640 and 1189 to 1643 and 1193 cm^{-1}, respectively). It indicates a stronger interplane $\pi-\pi$ interaction between the $V^{\bullet+}$ units, which is stabilized by van der Waals interactions within alkyl chains. A similar mechanism has been proposed to explain the blue shift of the B_{2u} vibrational band of V^{2+} at 1642 cm^{-1}. However, the ring vibrational bands of the dimer $(V^{\bullet+})_2$ do not shift, indicating that the vibronic coupling intensity is rather independent of the aliphatic environment. Such different trends of the chain length dependence suggest that the coupling between two subunits of a dimer is much stronger than the electrostatic $\pi-\pi$ interaction between neighboring monomeric $V^{\bullet+}$ radicals.[31−37,46]

Taking the intensity of the strongest monomer vibration around 1640 cm^{-1} as an internal standard, a more tilted orientation of the longer alkyl chains is suggested by the increased intensity of the N-R/N′-R dominated vibrational band around 1189 cm^{-1}. The relative intensities of the dimer modes at 1588 and 1507 cm^{-1}, with respect to that at 1640 cm^{-1}, increase with the length of the alkyl chain, indicating an increased preference of the dimerization in the following sequence: 6V6 < 8V8 < 10V10. Similar to the $\pi-\pi$ stacking between V^{2+} planes, the dimerization is also favored by the more tilted bipyridinium units connected to the longer alkyl chains.

3.2.2.3. Model of the $V^{\bullet+}$ Monolayer. Based on the above discussion, two schematic models of the $V^{\bullet+}$ adlayers were developed (Figure 8). Similar to the V^{2+} SAM, the van der Waals interactions between the long alkyl chains result in two aligned hydrophobic "sublayers", with the redox-active bipyridinium $V^{\bullet+}$ moiety enclosed. Both the monomers and the dimers of $V^{\bullet+}$ coexist in such a sandwich model. The alignment of the radical cations is stabilized by $\pi-\pi$ stacking between the monomers and a strong vibronic coupling within the dimers. The dimerization and the alignment are favored by the more tilted bipyridinium units. Both increase with the lengths of the alkyl chains.

4. Conclusions

We have reported a systematic electrochemical and in situ SEIRAS investigation of 6V6, 8V8, and 10V10 adlayers on electrified gold/aqueous electrolyte interfaces. The electrochemical experiments show that the first redox process $V^{2+} \leftrightarrow V^{\bullet+}$ is reversible, while the second redox process $V^{\bullet+} \leftrightarrow V^0$ is quasi reversible. The spectroscopic structure studies were focused on the V^{2+} and $V^{\bullet+}$ redox states.

The SAM of V^{2+} exhibits a sandwich-like structure: van der Waals interactions between alkyl chains lead to two hydrophobic

layers, with the redox-active bipyridinium V^{2+} layer enclosed in between. The alkyl chains are aligned in an all-trans configuration in a tilted orientation with some degree of conformational disorder. The long axis of the central bipyridinium rings is tilted with respect to the surface normal. The positive charge of the bipyridinium dications is balanced by the negatively charged anions located close to the annular nitrogen atoms. The alignment of V^{2+} is stabilized by interplanar $\pi-\pi$ interaction and electrostatic Coulombic interactions.

After reduction of $V^{2+} \rightarrow V^{\bullet+}$, radical cation monomers and dimers coexist within the adlayer. The alignment of the $V^{\bullet+}$ species is stabilized by the strong vibronic coupling within the dimers, as well as the $\pi-\pi$ stacking between monomers. The dimerization and the alignment are both favored by the more tilted bipyridinium units with an increase of alkyl chain lengths. The delocalization of radical electrons in the $V^{\bullet+}$ dimer increases the electronic transport through the adlayer, and supports the reductive switching characteristics recently observed in STM-based single molecule junction experiments with 6V6 and related molecules.[58,59]

Acknowledgment. The work was supported by the Volkswagen Foundation under grant no. I77−116, the HGF Project "Molecular Switches", the IFMIT, and the Research Center Jülich. We are indebted to Dr. G. Mészáros for his help and valuable suggestion to improve the electrochemical set-ups. The preparation of gold single crystals by U. Linke, and the assistance of H. Bierfeld in electron-beam evaporation are gratefully appreciated.

References and Notes

(1) Monk, P. M. S. *The Viologens*; John Wiley & Sons Ltd.: Chichester, England, **1998**; pp 1−52.
(2) Bird, C. L.; Kuhn, A. T. *Chem. Soc. Rev.* **1981**, *10*, 49−82.
(3) Terrill, R. H.; Hutchison, J. E.; Murray, R. W. *J. Phys. Chem. B* **1997**, *101* (9), 1535−1542.
(4) Jernigan, J. C.; Surridge, N. A.; Zvanut, M. E.; Silver, M.; Murray, R. W. *J. Phys. Chem.* **1989**, *93*, 4620−4627.
(5) Dalton, E. F.; Murray, R. W. *J. Phys. Chem.* **1991**, *95*, 6383−6389.
(6) Liu, X.; Neoh, K. G.; Cen, L.; Kang, E. T. *Biosens. Bioelectron.* **2004**, *19* (8), 823−834.
(7) Wang, X. J.; Dzyadevych, S. V.; Chovelon, J. M.; Renault, N. J.; Chen, L.; Xia, S. Q.; Zhao, J. F. *Electrochem. Commun.* **2006**, *8* (2), 201−205.
(8) Juan, Z.; Swager, T. M. *Adv. Polym. Sci.* **2005**, *177*, 151−179.
(9) Haramoto, Y.; Yin, M.; Matukawa, Y.; Ujiie, S.; Nanasawa, M. *Liq. Cryst.* **1995**, *19* (3), 319−320.
(10) Willner, I.; Eichen, Y.; Frank, A. J.; Fox, M. A. *J. Phys. Chem.* **1993**, *97* (28), 7264−7271.
(11) Sagara, T.; Kato, N.; Toyota, A.; Nakashima, N. *Langmuir* **2002**, *18* (18), 6995−7001.
(12) Yang, C. H.; He, G. F.; Wang, R. Q.; Li, Y. F. *Thin Solid Films* **2000**, *363* (1−2), 218−220.
(13) Haiss, W.; Van Zalinge, H.; Hörbenreich, H.; Bethell, D.; Schiffrin, D. J.; Higgins, S. J.; Nichols, R. J. *Langmuir* **2004**, *20*, 7694−7702.
(14) Gittins, D. I.; Bethell, D.; Schiffrin, D. J.; Nichols, R. J. *Nature* **2000**, *408*, 67−69.
(15) Lee, C.-W.; Bard, A. J. *J. Electroanal. Chem.* **1988**, *239*, 441−446.
(16) Lee, C.-W.; Bard, A. J. *Chem. Phys. Lett.* **1990**, *170*, 57−60.
(17) Raymo, F. M.; Alvarado, R. J.; Pacsial, E. J.; Alexander, D. *J. Phys. Chem. B* **2004**, *108*, 8622−8625.
(18) Raymo, F. M.; Alvarado, R. J.; Pacsial, E. J.; *J. Supramol. Chem.* **2002**, *2*, 63−67.
(19) Raymo, F. M.; Alvarado, R. J.; Giordani, S.; Cejas, M. A. *J. Am. Chem. Soc.* **2003**, *125*, 2361−2364.
(20) Alvarado, R. J.; Mukkerjee, J.; Pacsial, E. J.; Alexander, D.; Raymo, F. M. *J. Phys. Chem. B* **2005**, *109* (13), 6164−6173.
(21) De Long, H. C.; Buttry, D. A. *Langmuir* **1990**, *6*, 1319−1322.
(22) De Long, H. C.; Buttry, D. A. *Langmuir* **1992**, *8*, 2491−2496.
(23) Hiley, S. L.; Buttry, D. A. *Colloids Interfaces A* **1994**, *84*, 129−140.
(24) Sagara, T.; Maeda, H.; Yuan, Y.; Nakashima, N.; *Langmuir* **1999**, *15*, 3823−3830.
(25) Sagara, T.; Kaba, N.; Komatsu, M.; Uchida, M.; Nakashima, N.; *Electrochim. Acta* **1998**, *43*, 2183−2193.
(26) Sagara, T.; Tsuruta, H.; Nakashima, N. *J. Electroanal. Chem.* **2001**, *500*, 255−263.
(27) Wang, H. X.; Sagara, T.; Sato, H.; Niki, K. *J. Electroanal. Chem.* **1992**, *331* (1−2), 925−943.
(28) Sagara, T.; Miuchi, K. *J. Electroanal. Chem.* **2004**, *567* (2), 193−202.
(29) Sagara, T.; Tanaka, S.; Fukuoka, Y.; Nakashima, N. *Langmuir* **2001**, *17* (5), 1620−1629.
(30) Sagara, T.; Tanaka, S.; Miuchi, K.; Nakashima, N. *J. Electroanal. Chem.* **2002**, *524−525*, 68−76.
(31) John, S. A.; Kitamura, F.; Tokuda, K.; Ohsaka, T. *Electrochim. Acta* **2000**, *45* (24), 4041−4048.
(32) John, S. A.; Kitamura, F.; Tokuda, K.; Ohsaka, T. *J. Electroanal. Chem.* **2000**, *492* (2), 137−144.
(33) John, S. A.; Okajima, T.; Ohsaka, T. *J. Electroanal. Chem.* **1999**, *466* (1), 67−74.
(34) John, S. A.; Kasahara, H.; Okajima, T.; Tokuda, K.; Ohsaka, T. *J. Electroanal. Chem.* **1997**, *436* (1−2), 267−270.
(35) John, S. A.; Kitamura, F.; Tokuda, K.; Ohsaka, T. *Langmuir* **2000**, *16* (2), 876−880.
(36) John, S. A.; Ohsaka, T. *Electrochim. Acta* **1999**, *45* (7), 1127−1133.
(37) Arihara, M.; Kitamura, F.; Nukanobu, K.; Ohsaka, T.; Tokuda, K. *J. Electroanal. Chem.* **1999**, *473* (1−2), 138−144.
(38) Kim, J. H.; Lee, K. A. B.; Uphaus, R. A.; Cotton, T. M. *Thin Solid Films* **1992**, *210−211*, 825−827.
(39) Lu, T.; Cotton, T. M.; Hurst, J. K.; Thompson. D. H. P. *J. Phys. Chem.* **1988**, *92*, 6978−6985.
(40) Lu, T.; Cotton, T. M.; Hurst, J. K.; Thompson, D. H. P. *J. Electroanal. Chem.* **1988**, *246*, 337−347.
(41) Li, J.; Chen, G.; Dong, S. *Thin Solid Films* **1997**, *293*, 200−205.
(42) Lee, C.; Moon, M. S.; Park, J. W. *J. Electroanal. Chem.* **1996**, *407*, 161−167.
(43) Lee, C.; Lee, Y. M.; Moon, M. S.; Park, S. H.; Park, J. W.; Kim, K. G.; Jeon, S. J. *J. Electroanal. Chem.* **1996**, *416*, 139−144.
(44) Tang, X.; Schneider, T. W.; Buttry, D. A. *Langmuir*, **1994**, *10*, 2235−2240.
(45) Tang, X.; Schneider, T. W.; Walker, J. W.; Buttry, D. A. *Langmuir*, **1996**, *12*, 5921−5933.
(46) Osawa, M.; Suëtaka, W. *J. Electroanal. Chem.* **1989**, *270*, 261−272.
(47) Osawa, M.; Yoshii, K. *Appl. Spectrosc.* **1997**, *51* (4), 512−518.
(48) Osawa, M.; Yoshii, K.; Ataka, K.; Yotsuyanagi, T. *Langmuir* **1994**, *10* (3), 640−642.
(49) Ito, M.; Sasaki, H.; Takahashi, M. *J. Phys. Chem.* **1987**, *91*, 3932−3934.
(50) Sasaki, H.; Takahashi, M.; Ito, M. *Journal of Electron Spectr. Rel. Phen.* **1987**, *45*, 161−168.
(51) Brienne, S. H. R.; Cooney, R. P.; Bowmaker, G. A. *J. Chem. Soc. Faraday Trans.* **1991**, *87* (9), 1355−1359.
(52) Brienne, S. H. R.; Boyd, P. D. W.; Schwerdtfeger, P.; Bowmaker, G. A.; Cooney, R. P. *J. Chem. Soc. Faraday Trans.* **1993**, *89* (16), 3015−3020.
(53) John, S. A.; Ohsaka, T. *J. Electroanal. Chem.* **1999**, *477* (1), 52−61.
(54) Lee, C.; Lee, Y. K.; Lee, Y. M.; Jeon, I. C. *J. Electroanal. Chem.* **1999**, *463*, 224−231.
(55) Kaifer, A. E.; Gómez-Kaifer, M. *Supramolecular Electrochemistry*; Wiley-VCH: Weinheim, Germany, 1999; Chapter 9.
(56) Haiss, W.; Van Zalinge, H.; Higgins, S. J.; Bethell, D.; Hörbenreich, H.; Schiffrin, D. J.; Nichols, R. J. *J. Am. Chem. Soc.* **2003**, *125*, 15294−15295.
(57) Haiss, W.; Nichols, R. J.; Van Zalinge, H.; Higgins, S. J.; Bethell, D.; Schiffrin, D. J. *Phys. Chem. Chem. Phys.* **2004**, *6*, 4330−4337.
(58) Li, Z.; Han, B.; Meszaros, G.; Pobelov, I.; Wandlowski, T.; Błaszczyk, A.; Mayor, M. *Faraday Discuss.* **2006**, *131*, 121−143.
(59) Li, Z.; Pobelov, I.; Han, B.; Wandlowski, T.; Błaszczyk, A.; Mayor, M. *Nanotechnology* **2007**, *18*, 044018.
(60) Hölzle, M. H.; Wandlowski, T.; Kolb, D. M. *J. Electroanal. Chem.* **1995**, *394*, 271−275.
(61) Wandlowski, T.; Ataka, K.; Pronkin, S.; Diesing, D. *Electrochim. Acta*, **2004**, *49*, 1233−1247.
(62) Hartstein, A.; Kirtley, J. R.; Tsang, J. C. *Phys. Rev. Lett.* **1980**, *45*, 201−204.
(63) Pronkin, S.; Wandlowski, T. *J. Electroanal. Chem.* **2003**, *550−551*, 131−147.
(64) Bard, A. J.; Faulkner, L. R. *Electrochemical Methods: Fundamentals and Applications*, 2nd ed.; John-Wiley & Sons, Inc.: Hoboken, NJ, 2001; Chapter 6.
(65) Widrig, C. A.; Chung, C.; Porter, M. D. *J. Electroanal. Chem.* **1991**, *310*, 335−359.

(66) Finklea, H. O. *Electroanal. Chem.* **1996**, *19*, 109−335.
(67) Anson, F. C.; Blauch, D. N.; Saveant, J. M.; Shu, C. F. *J. Am. Chem. Soc.* **1991**, *113*, 1922−1932.
(68) Saveant, J. M. *J. Phys. Chem.* **1988**, *92*, 4526−4532.
(69) Monk, P. M. S.; Hodgkinson, N. M. *Electrochim. Acta* **1998**, *43* (3−4), 245−255.
(70) Creager, S. E.; Rowe, G. K. *Anal. Chim. Acta* **1991**, *246*, 233−239.
(71) Chidsey, C. E. D.; Bertozzi, C. R.; Putvinski, T. M.; Mujsce, A. M. *J. Am. Chem. Soc.* **1990**, *112* (11), 4301−4306.
(72) Kobayashi, K.; Fujisaki, F.; Yoshime, T.; Niki, K. *Bull. Chem. Soc. Jpn.* **1986**, *59*, 3715−3722.
(73) Russell, J. H.; Wallwork, S. C. *Acta. Cryst. B* **1972**, *28*, 1527−1533.
(74) Polishchuk, I. Y.; Grineva, L. G.; Polishchuk, A. P.; Chernega, A. N. *Russ. J. Gen. Chem.* **1996**, *66*, 1530−1536.
(75) Ulman, A. *Chem. Rev.* **1996**, *96*, 1533−1554.
(76) Flink, S.; Van Veggel, F. C. J. M.; Reinhoudt, D. N. *Adv. Mater.* **2000**, *12*, 1315−1328.
(77) Esplandiú, M. J.; Hagenström, H.; Kolb, D. M. *Langmuir* **2001**, *17*, 828−838.
(78) Han, B.; Li, Z.; Pronkin, S.; Wandlowski, T. *Can. J. Chem.* **2004**, *82* (10), 1481−1494.
(79) Arihara, K.; Kitamura, F. *J. Electroanal. Chem.* **2003**, *550*, 149−159.
(80) (a) Ghostal, S.; Lu, T.; Feng, Q.; Cotton, T. M. *Spectroelectrochim. Acta*, **1988**, *44A*, 651−660.
(81) Hester, R. E.; Suzuki, S. *J. Phys. Chem.* **1982**, *86*, 4626−4630.
(82) Duan, L.; Garrett, S. J. *Langmuir* **2001**, *17* (10), 2986−2994.
(83) Reipa, V.; Yeh, S. -M. L.; Monbouquette, H. G.; Vilker, V. L. *Langmuir* **1999**, *15* (23), 8126−8132.
(84) Rong, H. T.; Frey, S.; Yang, Y. J.; Zharnikov, M.; Buck, M.; Wühn, M.; Wöll, C.; Helmchen, G. *Langmuir* **2001**, *17*, 1582−1593.
(85) Porter, M. D.; Bright, T. B.; Allara, D. L.; Chidsey, C. E. D. *J. Am. Chem. Soc.* **1987**, *109*, 3559−3568.
(86) Nuzzo, R. G.; Dubois, L. H.; Allara, D. L. *J. Am. Chem. Soc.* **1990**, *112* (2), 558−569.
(87) Poirier, G. E. *Langmuir* **1997**, *13*, 2019−2026.
(88) Poirier, G. E. *Langmuir* **1999**, *15*, 1167−1175.
(89) Yang, G.; Liu, G. *J. Phys. Chem. B* **2003**, *107*, 8746−8759.
(90) Ulman, A.; Scaringe, R. P. *Langmuir* **1992**, *8* (3), 894−897.
(91) Shnidman, Y.; Ulman, A.; Eilers, J. E. *Langmuir* **1993**, *9* (4), 1071−1081.